Table 3 Results of 3rd- and 5th-order inner solutions

β	$\frac{2}{b^3}h''(0)$	$h'''(0)$	$h(\infty)$	$T''(0)$	$T'''(0)$	$T(\infty)$
0.05	7.831799	−1.129489	24.400880	...	...	...
0.1	3.342832	−0.892131	9.021522	626.100	−37.035363	877.868950
0.2	1.220751	−0.623236	2.538928	30.8200	−8.995353	25.521129
0.3	0.607804	−0.506658	0.971029	6.94458	−3.007645	3.802077
0.4	0.359899	−0.461224	0.421722	2.18406	−1.150627	0.779787
0.5	0.247636	−0.441216	0.197424	0.824847	−0.476491	0.165406
0.6	0.183200	−0.418365	0.090825	0.335752	−0.209822	−0.025134
0.8	0.129017	−0.295316	0.027121	...	...	...
0.9	0.081274	−0.172902	0.119886	...	...	...
0.95	0.046084	−0.093121	0.005844	...	...	...
1.00	0.0	0.0	0.0	...	...	...

In addition, the inner and outer solutions must match at $\eta = 0$ or $\sigma = \infty$ (outer boundary-layer limit) and the exponential decay of vorticity as $\sigma \to \infty$ must be met. These two conditions are given in Table 1.

Equation (1) can be reduced to an ordinary differential equation for solution via the Runge-Kutta Scheme if Ψ_i take special forms. These forms are

$$\Psi_2 = g(\sigma), \quad \Psi_3 = (1/b\xi)[h(\sigma)], \quad \Psi_4 = [1/(b\xi)^2]V(\sigma),$$
$$\Psi_5 = [1/(b\xi)^3][T(\sigma) - h(\infty)\sigma^2]$$

where g, h, V, and T are parameters to be calculated. The resulting ordinary differential equation and boundary conditions are given in Table 2.

In particular, g and V, which are governed by homogeneous equations and boundary conditions, were found to be zero. T, h, T', h' are zero at $\sigma = 0, T', h'$ and higher derivatives must vanish exponentially as $\sigma \to \infty$. Values of the initial conditions including $h(\infty)$ and $T(\infty)$ are given in Table 3.

The skin friction and pressure made dimensionless by $\frac{1}{2}\rho U(X)^2$ can be shown to be given by, respectively,

$$C_f = 2f''(0)/bR_X^{1/2} + 2h''(0)/b^3R_X^{3/2} + 2[T''(0) - 2h(\infty)]/b^5R_X^{5/2}$$

and

$$C_p = -h'''(0)/4\theta b^2R_X - T'''(0)/(2+4\theta)b^4R_X^2$$

where $R_X = [U(X)X/\nu]$ is based on local velocity at X. The dimensionless pressure does not include the inviscid pressure.

Conclusion

The results obtained here are not valid around the leading edge. The numerical solution of the Navier-Stokes equation which includes the leading edge has been found.[11] The skin-friction coefficient curves shown in Fig. 2 have been terminated as $R_X \to 0$. These curves approach the classical boundary-layer values as $R_X \to \infty$.

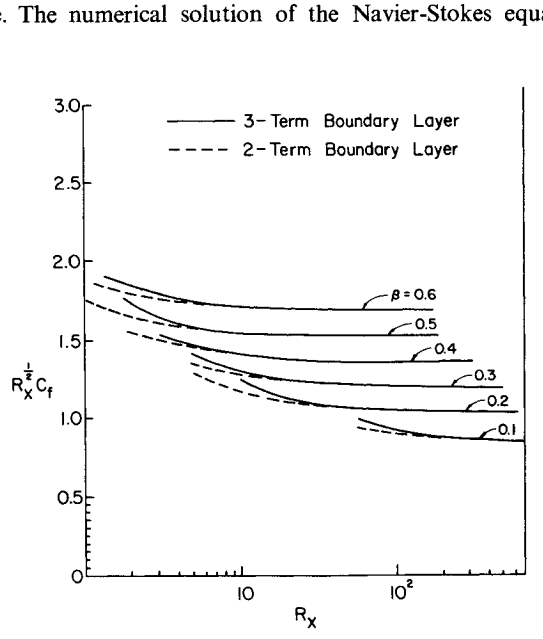

Fig. 2 Variations of $R_x^{1/2}C_f$ with R_x for the asymptotic solutions.

References

[1] Van Dyke, M., "Higher Order Boundary Layer Theory," *Applied Mechanics Review*, Vol. 1, 1969, pp. 265–292.

[2] Imai, I., "Second Approximation to the Laminar Boundary Layer Flow over a Flat Plate," *Journal of Aeronautical Sciences*, Vol. 24, 1957, pp. 155–156.

[3] Goldstein, S., *Lectures on Fluid Mechanics*, Wiley (Interscience), New York, 1960.

[4] Van de Vooren, A. and Dykstra, D., "Navier-Stokes Solution for Laminar Flow Past a Semi-Infinite Flat Plate," *Journal of Engineering and Mathematics*, Vol. 4, pp. 9–27.

[5] Rhyming, F., "On Viscous Wedge Flow," F.F.A. Rept. 116, Aeronautical Research Institute of Sweden, Stockholm, Sweden.

[6] Kaplun, S., "The Role of Coordinate Systems in Boundary Layer Theory," *Zeitschrift für Angewandte Mathematik und Physik*, Vol. 4, 1954, pp. 11–135.

[7] Faulkner, V. M. and Skan, S. W., "Some Approximate Solutions of the Boundary Layer Equations," R. and M. 1314, 1930, Aeronautical Research Council, London, England.

[8] Van Dyke, M., *Perturbation Methods in Fluid Mechanics*, Academic Press, New York, 1964.

[9] Hantree, D. R., "On an Equation Occurring in Faulkner-Skan Approximate Treatment of Equations of Boundary Layer," *Proceedings of the Cambridge Philosophical Society*, Vol. 33, pp. 223–239.

[10] Lagerstrom, P. A., *Laminar Flow Theory*, edited by F. K. Moore, Vol. 4 of *High Speed Aerodynamics and Jet Propulsion*, Princeton Univ. Press, Princeton, N.J., pp. 20–285.

[11] Evbuoma, S. N., "Analysis of Viscous Flow past Wedges at Low and Moderate Reynolds Numbers," Ph.D. thesis, 1973, University of Illinois, Urbana, Ill.

Contribution of a Wall Shear Stress to the Magnus Effect on Nose Shapes

IRA D. JACOBSON*
University of Virginia, Charlottesville, Va.

In recent years, several authors have calculated the Magnus effect on bodies of differing shapes[1-3] with either fully laminar or fully turbulent boundary layers. These analyses suggest that

Received December 26, 1973. The support of the Ballistic Research Laboratories, Aberdeen Proving Ground, Md., under Contract DAADOS-72-C0131 is gratefully acknowledged.

Index categories: Boundary Layers and Convective Heat Transfer—Turbulent; LV/M Aerodynamics.

* Assistant Professor, Department of Engineering Science and Systems. Member AIAA.

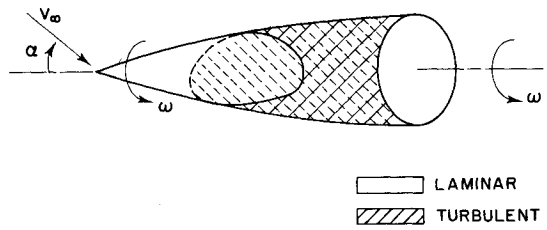

Fig. 1 Asymmetric boundary-layer transition.

the contribution of shear stress to the Magnus effect is small. The purpose of this Note is to illustrate that this effect may, in fact, not be small on nose shapes with mixed boundary layers (both laminar and turbulent) as is found in most experimental and flight conditions.[4] This case differs from the usual treatment of a fully laminar or fully turbulent flow where the resultant side force due to shear is a consequence of perturbations in the velocity field induced by angle of attack and spin. This causes an asymmetric distribution of the wall shear stress given by $\tau_x = \mu(du/dy)|_w$ for the axial component and $\tau_\phi = \mu(dw/dy)|_w$ for the azimuthal component. Thus the changes in τ_x and τ_ϕ over the surface of the body are at most small since they involve only small perturbations in the velocity field. On the other hand, for the case of a mixed boundary layer (Fig. 1), the differences in shear stress over the surface of the body are due not only to perturbations in the velocity field, but to the gross change in velocity slope at the wall for laminar vs turbulent flows. It is this case where the shear stress can make a significant contribution to the side force.

To illustrate this, consider the example of a 10° cone (the approach would be similar for other shapes as well). The side force due to axial shear can be written

$$F_y = \int_S C_f q_\infty l \sin^2\theta \sin\phi \, d\phi \, dl \tag{1}$$

where C_f is the axial skin-friction coefficient, q_∞ the dynamic pressure, θ the cone half-angle, ϕ the azimuthal angle, and l the distance along the surface of the cone. For incompressible flow, the skin-friction coefficients were calculated[3] using

$$C_{f\text{lam}} = \frac{1.19}{(V_\infty L/\nu)^{1/2}} \tag{2}$$

for laminar flow, and estimated[5] for turbulent flow as

$$C_{f\text{turb}} = \frac{0.036}{(V_\infty L/\nu)^{1/7}} \tag{3}$$

For the worst case, i.e., when the flow is completely laminar on one side of the body (port) and completely turbulent on the other (starboard), integration of Eq. (1) using Eqs. (2) and (3) yields a side force coefficient given by

$$C_y = F_y/q_\infty S = +[0.0123/(Re_L)^{1/7}] - [0.487/(Re_L)^{1/2}] \tag{4}$$

which has the value 0.0012 for $Re_L = 1 \times 10^6$ and 0.0011 for $Re_L = 1 \times 10^7$.

This can be compared to a side force due to displacement thickness for the fully laminar case of $-3 \times 10^{-2} * \alpha * (\omega R/V_\infty)$ for $Re_L = 1 \times 10^6$ and $-9.8 \times 10^{-3} * \alpha * (\omega R/V_\infty)$ for $Re_L = 1 \times 10^7$. For the mixed boundary-layer case, these will be slightly larger.[4] For small angles of attack and spin ratios [e.g., $\alpha = 0(0.1)$, $\omega R/V_\infty = 0(0.1)$], it can be seen that the shear contribution due to the mixed boundary layers can be as much as an order of magnitude greater than the displacement thickness contribution, and in the opposite direction.† Using a compressibility correction factor for the skin-friction coefficients[1] alters these slightly as shown in Table 1 for a Reynolds number of 5×10^6.

An even more important effect than this difference in side force is the moment generated by the shear stress. For the case of a cone, the moment center is the apex—which gives the largest possible moment arm. If the cone is the nose shape used on a larger configuration, it is reasonable to assume that an asym-

Table 1 Effect of Mach number on side force due to axial shear

M	C_y
0	0.0011
2	0.0013
3	0.0014

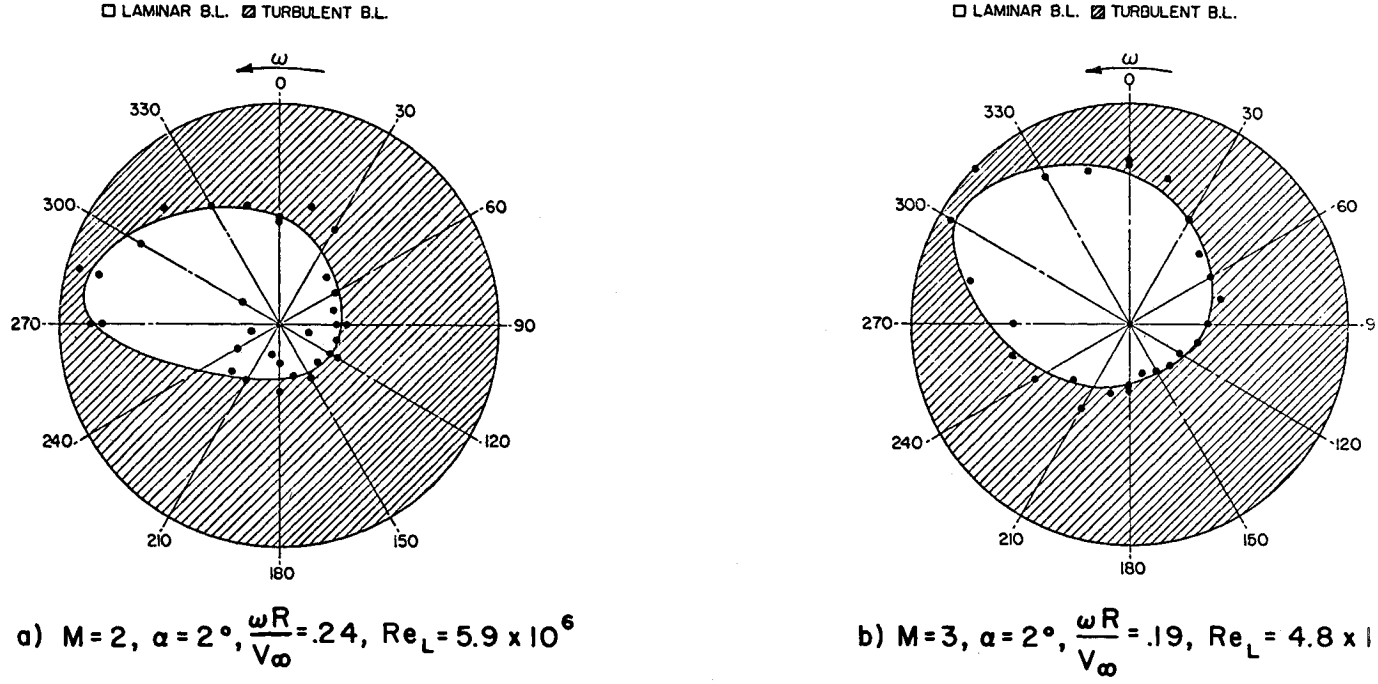

Fig. 2 Profile of boundary-layer transition on a 10° half-angle cone.

† It is important to recognize that this is at best an estimate since the Mangler transformations and compressibility corrections used do not apply in turbulent regions, and the velocity profile for turbulent flow on a spinning body at angle of attack is not known.

Table 2 Comparison of contributions to Magnus side force coefficient

	C_y (pressure dist.)[6]	C_y (axial shear)	C_y (measured)[6]
Case I	−0.0023	0.0006	−0.0002
Case II	−0.0016	0.0005	−0.0008

metric transition pattern on the nose will contribute significantly to the Magnus moment.

To estimate the significance of this effect for an actual 10° half-angle cone, the contribution due to the pressure field (displacement effect) and axial shear stress are compared using data from Ref. 6. The magnitudes of the calculated terms are shown in Table 2 for two cases: Case I—Mach number = 2, $\alpha = 2$, $Re_L = 5.9 \times 10^6$, $\omega R/V_\infty = 0.24$; and Case II—Mach number = 3, $\alpha = 2$, $Re_L = 4.8 \times 10^6$, $\omega R/V_\infty = 0.19$, along with the measured value of the side force coefficient. The measured transition profiles are shown in Fig. 2.

It can be seen here that the shear contribution is a significant portion of the total and corrects the force in the proper direction for comparison with the measured data but appears to be too small for both cases, especially for Case I. Considering the data uncertainties and the assumptions involved in the shear force calculation, the trend is encouraging.

Thus, it has been shown that the shear contribution to the Magnus force and moment can be significant on nose shapes where a mixed asymmetric boundary layer exists, and a method of estimation indicated.

References

[1] Vaughn, H. R. and Reis, G. E., "A Magnus Theory for Bodies of Revolution," SC-RR-720537, Jan. 1973, Sandia Labs., Albuquerque, N. Mex.

[2] Sedney, R., "Laminar Boundary Layers on a Spinning Cone at Small Angles of Attack in a Supersonic Flow," *Journal of Aeronautical Science*, June 1957, pp. 430–436.

[3] Jacobson, I. D., Vollmer, A. G., and Morton, J. B., "Calculations of the Velocity Profiles of the Incompressible Laminar Boundary Layer on a Yawed Spinning Cone and the Magnus Effect," BRL CR-110, July 1973, Ballistic Research Labs., Aberdeen Proving Ground, Md.

[4] Jacobson, I. D., "Magnus Characteristics of Arbitrary Rotating Bodies," AGARDograph, Dec. 1973.

[5] Monin, A. S. and Yaglon, A. M., "Statistical Fluid Mechanics," *Mechanics of Turbulence*, M.I.T. Press, Cambridge, Mass., 1971.

[6] Sturek, W. B., "Boundary Layer Studies on a Spinning Cone," BRL-1649, May 1973, Ballistic Research Labs., Aberdeen Proving Ground, Md.

Calculation of Low Reynolds Number Flow past a Square Protuberance

CLARENCE W. KITCHENS JR.

Ballistic Research Laboratories, Aberdeen Proving Ground, Md.

Introduction

THE qualitative features of the flowfield downstream of two-dimensional roughness elements immersed in a laminar flat plate boundary layer are well known. Such protuberances are employed in many wind-tunnel experiments to promote transition and assure turbulent boundary-layer characteristics on models. Sedney[1] has described the effects of two- and three-dimensional protuberances on boundary-layer flows. In the two-dimensional case at low speeds, transition generally occurs downstream of the reattachment point if the protuberance height k is considerably less than the undisturbed boundary-layer thickness δ.

This Note describes numerical solutions of the steady-state Navier-Stokes equations for the flowfield near a square two-dimensional protuberance immersed in a plane Couette flow. We expect some of the qualitative features of the separation phenomena induced by the protuberance in the Couette flow to be similar to those found in the flat plate boundary-layer case. Numerical results have been obtained for Reynolds numbers, Re, between 1 and 200 based on plate velocity and protuberance height.

Description of Numerical Calculations

The steady-state Navier-Stokes equations for incompressible flow can be expressed in rectangular coordinates in terms of the vorticity transport equation

$$\frac{\partial}{\partial x}\left(\zeta\frac{\partial\psi}{\partial y}\right)-\frac{\partial}{\partial y}\left(\zeta\frac{\partial\psi}{\partial x}\right)-\nu\left(\frac{\partial^2\zeta}{\partial x^2}+\frac{\partial^2\zeta}{\partial y^2}\right)=0 \tag{1}$$

and a Poisson equation

$$(\partial^2\psi/\partial x^2)+(\partial^2\psi/\partial y^2)+\zeta=0 \tag{2}$$

where vorticity ζ is defined by

$$\zeta=(\partial v/\partial x)-(\partial u/\partial y) \tag{3}$$

and stream function ψ is defined to satisfy the continuity equation

$$u=\partial\psi/\partial y \quad \text{and} \quad v=-\partial\psi/\partial x \tag{4}$$

Numerical solutions of Eqs. (1) and (2) have been obtained using a Gauss-Seidel iteration procedure. The solution technique is based on a method developed by Gosman et al.[2] using an upwind difference scheme to approximate the convective terms.

Figure 1 shows a schematic of the computational region and boundary conditions employed in the numerical calculations. Plate EF moves at constant speed U_o above the stationary plate and protuberance ABCD. Vorticity boundary conditions along the stationary or moving walls are obtained by a Taylor series expansion of the stream function in terms of the mesh spacing normal to the wall ($\Delta\eta$), where ψ_w represents the stream function along the wall and ψ_{w+1}, the value at the grid point adjacent to the wall. Results shown in this Note are based on a second-order accurate equation for the wall vorticity

$$\zeta_w=-\frac{3}{(\Delta\eta)^2}[\psi_{w+1}-\psi_w-(\Delta\eta)U_o]-\frac{\zeta_{w+1}}{2}+0(\Delta\eta^2) \tag{5}$$

which is valid for a stationary wall when U_o is set equal to zero. Calculations were also performed using a first-order accurate equation for wall vorticity with little difference in the results.

Two different grid mesh configurations were used in the calculations. The grid consisted of a 6×11 cell protuberance immersed in a 51×21 cell flowfield for $Re \leqq 50$, with a larger 81×21 cell flowfield used for $Re \geqq 100$. The upstream boundary. AE, was located at approximately $X=-8$ for all Re, where

$$X=(x-x_k)/k \tag{6}$$

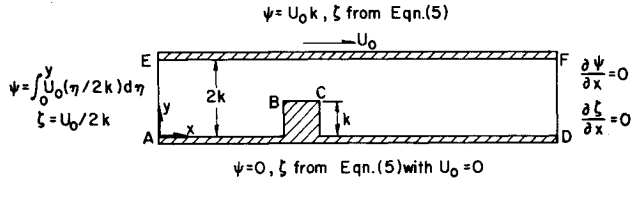

Fig. 1 Schematic of computational region and boundary conditions.

Presented at the Open Forum Session of the AIAA Computational Fluid Dynamics Conference, Palm Springs, Calif., July 19–20, 1973; received January 28, 1974.

Index categories: Boundary-Layer Stability and Transition; Hydrodynamics; Viscous Nonboundary-Layer Flows.

* Aerospace Engineer, Exterior Ballistics Laboratory. Member AIAA.